

PACS numbers: 31.30.Gs; 32.60.+i; 32.70.–n
DOI: 10.1070/QE2015v045n07ABEH015562

Observation of narrow isotopic optical magnetic resonances in individual emission spectral lines of neon

E.G. Saprykin, V.A. Sorokin, A.M. Shalagin

Abstract. **Narrow resonances are observed in the course of recording the individual emission lines of the glow discharge in the mixture of isotopes ^{20}Ne and ^{22}Ne, depending on the strength of the longitudinal magnetic field. The position of resonances in the magnetic scale corresponds to the compensation of the isotopic shift for certain spectral lines due to the Zeeman effect. It is found that the contrast of the resonances is higher for the transitions between the highly excited energy levels, and the resonances themselves are formed in the zone of longitudinal spatial nonuniformity of the magnetic field.**

Keywords: *neon, isotopes, optical magnetic resonances, collective spontaneous emission.*

1. Introduction

The authors of [1–4] reported the observation of unusual optical magnetic resonances (OMRs) in the mixture of even isotopes of neon. In the course of recording the intensity of radiation from the glow discharge in the gas mixture, consisting of the ^{20}Ne and ^{22}Ne atoms, depending on the magnetic field strength, the narrow low-contrast structures were observed. The glow observation was performed in the axially symmetric geometry: the direction of the magnetic field coincided with the direction of the current in the gas-discharge cell; the glow of the discharge, propagating along the cell axis, was recorded; and the recorded radiation was not spectrally selected at all, except the crude selection by means of coloured glasses in some cases.

Analysing the experimental results, it was established [1–4] that the formation of OMRs is closely related to the simultaneous presence of both isotopes of neon in the gas mixture, and the OMR position in the scale of the magnetic field strengths is caused by the Zeeman compensation of the isotopic frequency shift of certain transitions. In the process of collective spontaneous photoemission the resonance character of the interaction between the atoms, belonging to different isotopes, manifested itself in the formation of OMRs with the widths, much smaller than the Doppler one. In Ref. [3] the assumptions about the nature of the effect as a manifestation of collective spontaneous emission by pairs of closely spaces atoms of different isotopes were reported. The theoretical substantiation of this hypothesis is presented in a number of papers (see references in [3]).

In the present paper we report the observation of similar resonances in the emission of individual spectral lines in the visible spectral region and analyse their properties.

E.G. Saprykin Institute of Automation and Electrometry, Siberian Branch, Russian Academy of Sciences, prosp. Akad. Koptyuga 1, 630090 Novosibirsk, Russia; e-mail: Saprykin@gorodok.net;
V.A. Sorokin, A.M. Shalagin Institute of Automation and Electrometry, Siberian Branch, Russian Academy of Sciences, prosp. Akad. Koptyuga 1, 630090 Novosibirsk, Russia; Novosibirsk State University, ul. Pirogova 2, 630090 Novosibirsk, Russia; e-mail: vlad_sorokin@ngs.ru, Shalagin@iae.nsk.su

Received 20 May 2014; revision received 5 July 2014
Kvantovaya Elektronika **45** (7) 672–679 (2015)
Translated by V.L. Derbov

2. Experiment

The technique of the measurements and the used instrumentation are analogous to those described in Refs [1–4]. The registration geometry is described in detail in Ref. [5]. The difference is the use of the MDR-2 monochromator for selecting the radiation of individual neon lines. The radiation from the gas discharge cell was entered into the MDR-2 monochromator by means of an ordered optical waveguide. The entrance window of the optical waveguide was coincident with the focal plane of the objective, having the focal length $F \approx 60$ mm and focusing the radiation from the gas-discharge cell. The exit window of the optical waveguide and the slit of the monochromator were located in the conjugate planes of the focusing lens (condenser) with $F \approx 50$ mm. The exit window of the optical waveguide was imaged onto the input slit with triple demagnification in order to optimise the filling of the collimator objective of the monochromator with light and to reduce the image of the light source at the entrance slit. To perform the spectral selection we used the reflecting diffraction grating (600 grooves mm^{-1}) in the first order of diffraction with the operating spectral range from 400 to 1200 nm. The spectra were recorded in the range 533.1–878.4 nm, which made it possible to eliminate the additional spectral filters and to avoid the overlapping of the diffraction orders of the grating. By means of the aspheric lens the radiation output from the monochromator was sent to the photosensitive element of a silicon photodiode. The diode photocurrent was transformed into the output voltage by means of the inverting current-to-voltage converter with the feedback resistance 6.8 GΩ and the input current smaller than 0.1 pA. The photodetector sensitivity threshold was $\sim 1.1 \times 10^{-15}$ W Hz$^{-1/2}$. The slope of the photodetector sensitivity curve amounted to 0.67 nV (quantum s^{-1})$^{-1}$ for visible radiation with the wavelength $\lambda = 0.8$ μm (in the maximum of the photodiode spectral sensitivity).

The registration of the glow from the cell was implemented using two methods. The optical magnetic contour (OMC), i.e., the dependence of the glow-discharge radiation intensity (the photodetector output signal) on the strength of

the longitudinal magnetic field, was measured. Simultaneously the derivative of the OMC (DOMC) was measured. The method of DOMC measurement was based on the modulation of the magnetic field at the frequency ~70 Hz by means of an additional solenoid with subsequent synchronous detection of the alternating component of the photodetector output signal. The OMC and DOMC were stored in the digital form, which allowed essential improvement of the signal-to-noise ratio in the case of multipass scanning of the magnetic field with digital data acquisition.

3. Results of the measurements

Figure 1 presents the examples of DOMC, recorded for individual neon lines, belonging to the transitions of the 2p–1s multiplet. All plots were subject to a certain correction removing their slope. This procedure is equivalent to subtracting the low-informative parabolic envelope from the initial OMC, which allows some enhancement of the visual contrast of resonances. Besides that, all plots were reduced to the same scale and were vertically separated for clarity. The abscissa axis displays the mean magnetic field in the cell, which was determined with the distribution profiles of the scanned and modulating magnetic fields taken into account:

$$H = 0.4\pi i N_s \frac{\int_0^L G_s(z)\, G_m(z)\, dz}{\int_0^L G_m(z)\, dz}.$$

Here i is the current in the scanned solenoid coil; N_s is the winding density of the scanned solenoid (the number of turns per centimetre); $G_s(z)$ and $G_m(z)$ are the profiles of the field along the z axis for the scanned and modulating solenoids [see plots (*1*) and (*6*) in Fig. 6b]; and the integration limits correspond to the discharge boundaries. The magnetic field strength values present in all figures below were determined in a similar way.

Totally the 2p–1s multiplet consists of 25 allowed electric dipole transitions, and only for some of them ($2p_1-1s_4$, $2p_1-1s_2$, $2p_2-1s_5$, $2p_2-1s_2$, $2p_3-1s_2$, $2p_4-1s_2$) we could observe the least manifestations of the resonance behaviour of the DOMC during the reasonable recording time. It is worth noting that curve (*7*) in Fig. 1 corresponds to the line with the wavelength 672.5 nm*, which is not a neon spectral line and, most probably, belongs to the spectrum of atomic oxygen [6]. All lines of the 2p–1s multiplet were sufficiently intense, but in the interval of the magnetic field strength values 1200–1400 Gs the OMCs, visible against the noise background, were observed only for the transition lines $2p_1-1s_4$ and $2p_3-1s_2$. Below in the text these resonances are referred to as OMR-1200. For the rest lines the OMR-1200 amplitudes did not exceed the noise level. Thus, the amplitudes and the contrast of resonances, recorded at the lines of the multiplet 2p–1s, appeared to be significantly larger than those observed in the spectrally integral radiation [1–3]. That is why it was decided to measure the OMC and DOMC at the lines, corresponding to the transitions between higher excited energy levels.

Figure 2 presents the DOMC plots, corresponding to the transitions to the 2p energy sublevels from higher excited states. The raw curves were processed using the similar techniques as the plots in Fig. 1. The DOMC contain essentially more contrast resonances as compared to the data obtained at the transitions of the 2p–1s multiplet. The highest-contrast resonances are also centred at the magnetic field strength 1200–1400 Gs (OMR-1200). The vertical lines in Fig. 2 correspond to the expected positions of the isotopic resonances, calculated in Ref. [3]. The DOMC at the lines 533.07775, 576.44188, and 886.57562 nm, besides the sharp structures, contained weakly expressed parabolic 'pad'. The OMR-1200 at the line 576.44188 nm was observed virtually without any background. The OMR-1200 could be also observed in the OMC, but with a significantly smaller contrast. Nevertheless, it was quite sufficient to determine the OMR sign, which appeared to be negative, i.e., corresponding to a decrease of the discharge glow intensity, similar to Ref. [3].

A significantly higher OMR-1200 contrast for the transitions between the highly excited energy levels allowed the quantitative measurements of their parameters. Figure 3 pres-

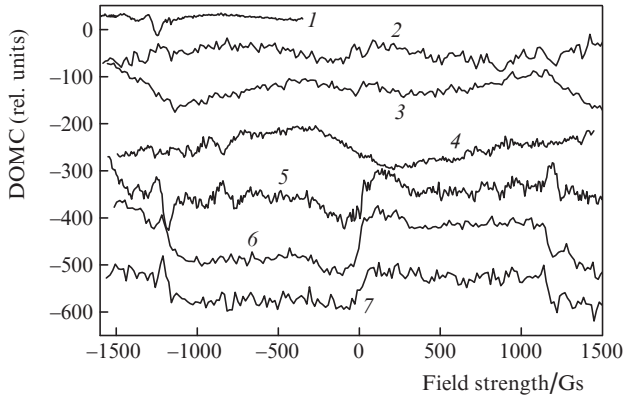

Figure 1. DOMC at the lines of neon, belonging to the multiplet 2p–1s: (*1*) λ = 540.05616 nm, $2p_1-1s_4$, oscillator strength f = 0.0004; (*2*) λ = 585.24878 nm, $2p_1-1s_2$, f = 0.0833; (*3*) λ = 588.18950 nm, $2p_2-1s_5$, f = 0.0368; (*4*) λ = 659.89529 nm, $2p_2-1s_2$, f = 0.145, (*5*) λ = 665.20925 nm, $2p_3-1s_2$, f = 0.00093; (*6*) λ = 667.82764 nm, $2p_4-1s_2$, f = 0.249, (*7*) λ = 672.5 nm, atomic oxygen. The spectroscopic parameters of the lines are given in Paschen notations.

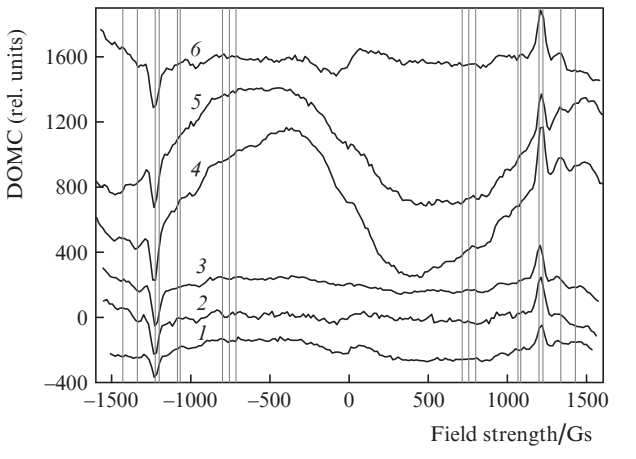

Figure 2. DOMC at the neon lines belonging to the transitions to the 2p levels from higher excited states: (*1*) λ = 886.57562 nm, $3d_4-2p_6$; (*2*) λ = 533.07775 nm, $4d_3-2p_{10}$, (*3*) λ = 57644188 nm, $4d'_4-2p_9$; (*4*) λ = 753.57739 nm, $3d_5-2p_{10}$; (*5*) λ = 878.37539 nm, $3s_1-2p_2$; (*6*) λ = 582.01558 nm, $4d_4-2p_8$. Vertical lines show the positions of possible isotopic resonances.

* The nearest spectral lines of substances: 672.4476 nm – CsI, 672.456 nm – CII, 672.6283 nm – OI, 6726478 nm – FeI, 672.6538 nm – OI.

ents three series of curves, obtained at the neon lines 878.37539, 57644188 and 533.07775 nm with the discharge current varied from 30 to 90 mA. The measurement technique for each of the lines was the same. The series began from the discharge current 90 mA. In each consequent record the current was decreased by 15 mA. The last record of the series was performed with the 90 mA current again. In Fig. 3 the beginning and the end of the series are curves (*1*), demonstrating the stability and reproducibility of the measurement results. For all resonances, centred at ±(1200–1400) Gs the increase in the discharge current was accompanied by the growth of the resonance amplitude up to the maximal value followed by a further decrease. Minor variations of the OMR positions were also observed. The shape of the OMR remained rather asymmetric.

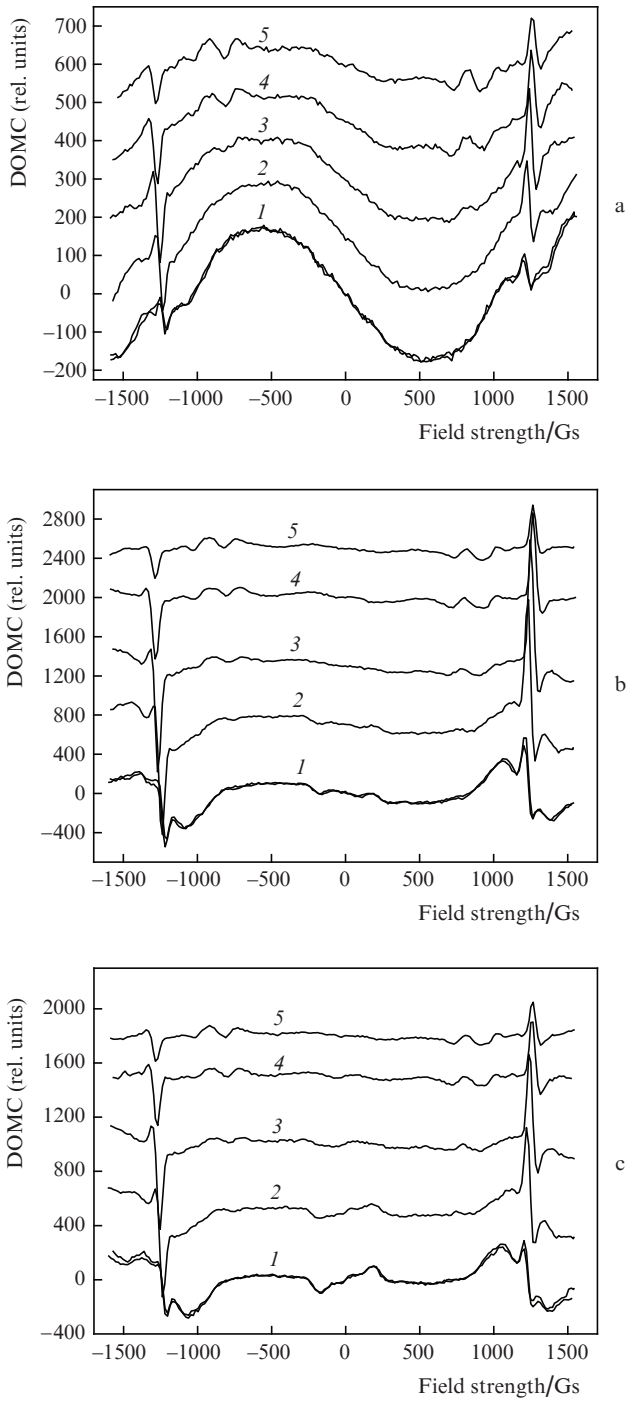

Figure 3. DOMC at the neon lines with (a) $\lambda = 878.37539$ nm, $3s_1-2p_2$; (b) $\lambda = 576.44188$ nm, $4d_4'-2p_9$; (c) $\lambda = 533.07775$ nm, $4d_3-2p_{10}$ for the discharge current (*1*) 90, (*2*) 75, (*3*) 60, (*4*) 45 and (*5*) 30 mA.

For the quantitative determination of the OMR-1200 parameters (amplitude, shift, width) from each DOMC two resonance-containing fragments were extracted. Then, using the maximum likelihood method, each fragment was approximated with a resonance function F_{res} obtained in Ref. [5] for the magnetic field, having along the z axis a continuous profile consisting of two regions. In the first region the field strength linearly grows along the axis from H_{min} to H_{max}. In the second region the field is uniform, and its strength equals H_{max}. The OMR shape for the uniform field is assumed to be Lorentzian:

$$F_{res}(A, K_a, q, \Delta, \Gamma, x) = A\left\{\frac{\Gamma^2}{\Gamma^2 + (x-\Delta)^2} + \right.$$
$$\left. + \frac{K_a}{x\Gamma^{-1}(1-q)}\left[\arctan\left(\frac{x-\Delta}{\Gamma}\right) - \arctan\left(\frac{xq-\Delta}{\Gamma}\right)\right]\right\}.$$

Here A is the resonance amplitude; Γ is the width of the resonance; Δ is the shift of the resonance; K_a is the relative contribution of the region where the magnetic field is nonuniform; $q = H_{min}/H_{max}$ is the parameter that determines the relative value of the nonuniformity of the magnetic field distribution; and x is the effective strength of the magnetic field, proportional to the current in the scanned solenoid. The function F_{res} contains two terms, one of them Lorentzian, symmetric with respect to Δ, and the other one asymmetric, containing the arctan functions (at $q = 1$ this part of the F_{res} turns into a Lorentzian). The total approximating function F_{ap}, besides the derivative of F_{res}, contains the pad function F_p that describes the DOMC envelope in the region of the resonance localisation:

$$F_{ap} = F_p(x) + \frac{d}{dx}F_{res}(A, K_a, q, \Delta, \Gamma, x).$$

Figures 4a–c present the dependences of the amplitudes, shifts and widths of the OMR-1200 on the discharge current. For comparison with Fig. 4a, Fig. 4d shows the dependences of the intensity of the corresponding spectral lines on the discharge current. The intensity measurements were carried out with the magnetic field strength values ±1200 Gs. Figure 4d presents their averaged values. The dependences of amplitudes and widths are shown separately for each sign of the magnetic field; for the shifts the averaging was applied. In the process of averaging the sign of the negative shifts was changed. The errors in determining the parameters, indicated in the figures, are statistical and do not allow for the errors of magnetic field calibration, the precision of which is better than 1%. The basic regularities of the behaviour of OMR parameters are as follows. With increasing discharge current a noticeable decrease in the OMR-1200 shift and a certain reduction of the resonance widths are observed. The OMR-1200 amplitudes at first increase with the growth of the discharge current and reach the maximal value, and then decrease, although the intensities of the corresponding spectral lines only grow.

Figure 5 presents the DOMC for the line at 576.44199 nm, demonstrating the effect of the additional magnetic field on the regions of the gas-discharge cell near to the photodetector

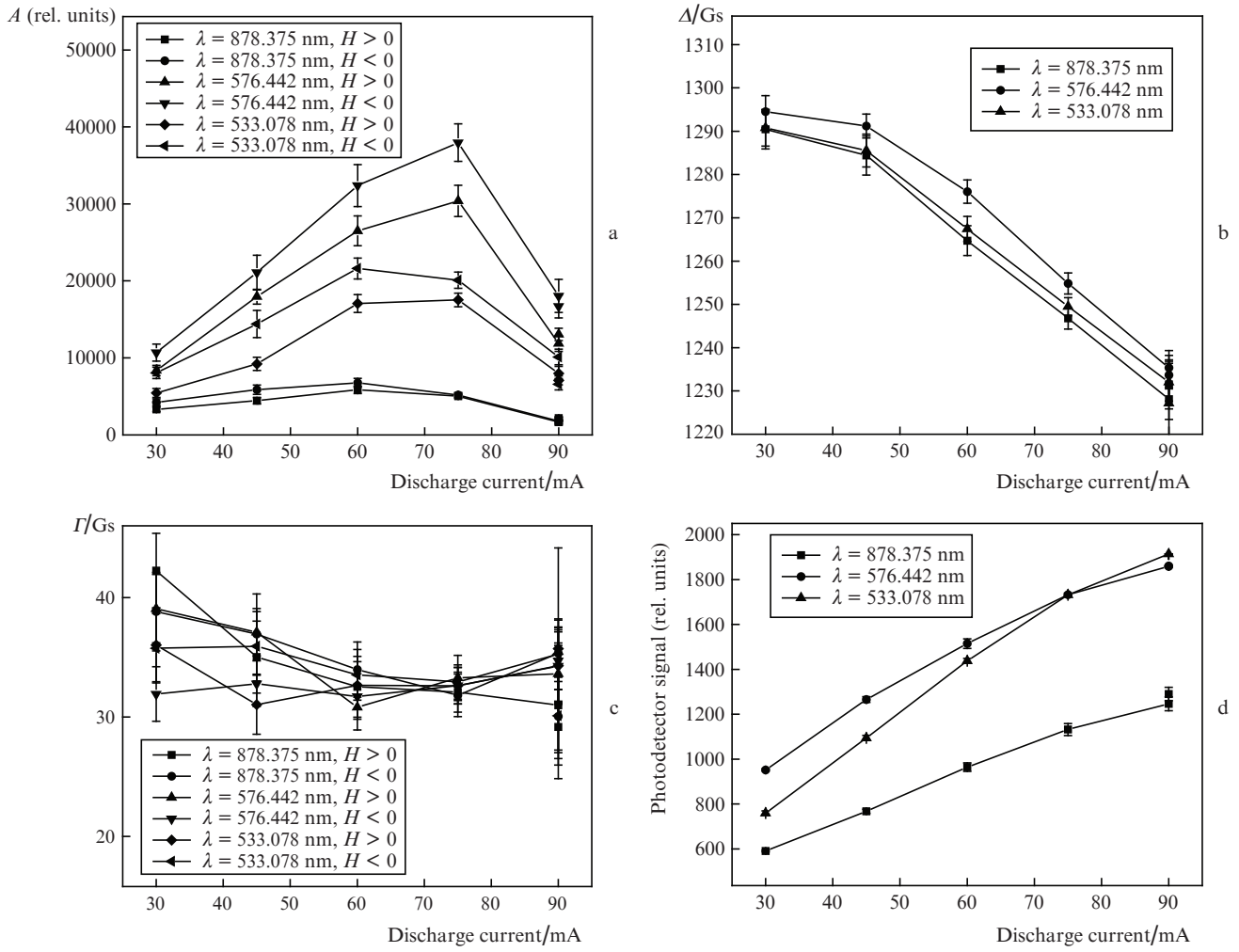

Figure 4. Parameters of OMR-1200 (a–c) and the photodetector signal (b, d) versus the discharge current; $H = \pm 1200$ Gs.

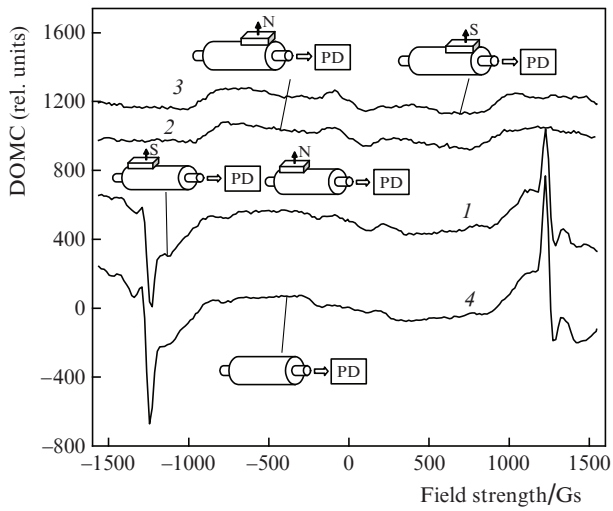

Figure 5. DOMC at the neon line with $\lambda = 576.44188$ nm under the action of the additional transverse magnetic field on different regions of the gas discharge cell (*1–3*) and in the absence of the additional field (*4*).

and far from it. The additional field was produced by the permanent magnet, having the shape of a rectangular parallelepiped with the dimensions 80×120×15 mm. The magnet was placed on the surface of the scanned solenoid, schematically shown in Fig. 5, at the distance 5.5 cm from the cell axis. On the surface of the magnet the field is perpendicular to the 80×120 mm face and is similar to the field of a rectangular current-conducting coil, having similar dimensions. Near the cell axis the additional field had both transverse and the longitudinal components. The maximal value of the transverse component was ~280 Gs, and the maximal absolute value of the longitudinal component was ~120 Gs.

The action of the additional magnetic field is reduced to two basic effects, namely, the complete disappearance of the narrow OMR-1200 under the application of the additional transverse field of any sign to the end of the cell nearer to the photodetector [curves (*2*) and (*3*) in Fig. 5], and the absence of essential influence of the additional transverse magnetic field applied to the end of the cell, located far from the photodetector, on the shape of the OMR-1200 [curve (*1*) in Fig. 5].

4. Discussion of the results

According to the hypothesis formulated in Ref. [3], the resonance features of the OMC in the region 1200–1400 Gs should be related to the transitions $2p_5-1s_5$ (1225 Gs), $2p_{10}-1s_5$ (1200 Gs) and $2p_5-1s_4$ (1338 Gs). However, the registration of the discharge glow directly at these transitions did not reveal OMR-1200. The only line ($\lambda = 588.18950$ nm, $2p_2-1s_5$)

with the lower metastable level $1s_5$, at which the DOMC has a weakly expressed resonance [curve (*3*) in Fig. 1], corresponds to the transition between the primed and non-primed terms with the small value of the oscillator strength ($3p'[1/2]$, $J_m = 1 - 3s[3/2]^0$, $J_n = 2^{**}$; $f = 0.0368$). The emission resonance at other transitions of the 2p–1s multiplet also appeared to be very low-contrast (see Fig. 1). For the curves, presented in Fig.1, the most contrast OMR-1200 are those for the line with $\lambda = 540.05616$ nm [the transition $3p'[1/2]$, $J_m = 0 - 3s[3/2]^0$, $J_n = 1$, ($2p_1 - 1s_4$); $f = 0.0004$, curve (*1*)], as well as for the line with $\lambda = 665.20925$ nm [$3p'[1/2]$, $J_m = 0 - 3s'[1/2]^0$, $J_n = 1$ ($2p_3 - 1s_2$); $f = 0.00093$, curve (*5*)] with the minimal values of the oscillator strength.

The suppression of the OMR-1200 signal is, probably, due to the absorption of radiation by the region of the discharge volume nearly 4 cm long that is out of the zone of the magnetic field action. The behaviour of the resonances for strongly absorbing transitions can be understood basing on the one-dimensional transfer equation for inhomogeneous medium:

$$\frac{dI}{dz} + \kappa(z) I = D(z). \tag{1}$$

Here $I = I(z)$ is the light intensity at the point with the coordinate z; $\kappa(z)$ is the absorption coefficient; and $D(z)$ is the luminosity of the layer at the point with the coordinate z.

The general solution of Eqn (1) has the form of a sum of contributions from individual layers, with the absorption of light on its path to the photodetector taken into account:

$$I(L) = \int_0^L D(z_1) \exp\left[-\int_{z_1}^L \kappa(z_2)\, dz_2\right] dz_1,$$
$$D(z) = A_r[1 + \alpha\varphi(H)],\ \kappa(z) = B_r[1 + \beta\varphi(H)],\ H = H(z). \tag{2}$$

Here A_r and B_r are proportional to the first and second Einstein coefficients; $\varphi(H)$ describes the shape of the OMR; and L is the length of the gas discharge gap. The parameters $\kappa(z)$ and $D(z)$ have the parts, independent of the magnetic field strength and dependent on it, and the dependence on z is determined by the function $H(z)$. Let us assume the contrast of resonances to be small ($\alpha \ll 1$ and $\beta \ll 1$). If the medium consists of two homogeneous layers, one of them with the thickness L_H located in the magnetic field and the other one out of the field, then the difference in absorption coefficients and radiation parameters for these layers is reduced to the presence or absence of the dependence on H in $\kappa(z)$ and $D(z)$. Then, solution (2) can be written in the form:

$$I(L) = \frac{D_1}{k_1}[1 - \exp(-k_1 L_H)]\exp[-k_2(L - L_H)] + \frac{D_2}{k_2}\exp[-k_2(L - L_H)],$$

$$\kappa(z) = \begin{cases} k_1 = B_r[1 + \beta\varphi(H)], & 0 < z \leqslant L_H, \\ k_2 = B_r, & L_H < z \leqslant L, \end{cases} \tag{3}$$

$$D(z) = \begin{cases} D_1 = A_r[1 + \alpha\varphi(H)], & 0 < z \leqslant L_H, \\ D_2 = A_r, & L_H < z \leqslant L, \end{cases}$$

from which it is easy to see the origin of the exponential attenuation of the magnetic field-dependent part of the emission from the cell due to the light absorption at the interval from L to L_H.

The formation of high-contrast resonances at the transitions between the highly excited levels can be studied by the example of a three-level cascade system with the energy levels n_1, n_2, n_3 (n_1 corresponding to the maximal energy and n_3 to the minimal one). The balance of populations is described by the system of differential equations:

$$\frac{dN_1}{dt} + \Gamma_1 N_1 = Q_1 + S_{21} N_2,$$
$$\frac{dN_2}{dt} + \Gamma_2 N_2 = Q_2 + A_{12} N_1 + S_{32} N_3, \tag{4}$$
$$\frac{dN_3}{dt} + \Gamma_3 N_3 = Q_3 + A_{23} N_2.$$

Here N_j ($j = 1, 2, 3$) is the population of the level n_j; Q_j is the corresponding excitation rate; A_{12} and A_{23} determine the increase in the population of the levels n_2 and n_3 due to the spontaneous emission of atoms, populating the levels n_1 and n_2, respectively; S_{21} and S_{32} determine the increase in the population of the levels n_1 and n_2 at the expense of the light absorption processes; and $\Gamma_1 = \Gamma_{10} + A_{12}$, $\Gamma_2 = \Gamma_{20} + A_{23}$ and Γ_3 determine the decrease in the population of the appropriate levels n_j, whereas Γ_{10} and Γ_{20} describe the contribution to this decrease in the transitions from the levels n_1 and n_2 to all levels, different from n_2 and n_3, respectively. Let us assume that the conditions for the formation of resonances arise at the 'lower' transition n_2, n_3 in the form of small additions to A_{23} and S_{32} ($A_{23} = A_{23} + \alpha_{23}$, $S_{32} = S_{32} + \sigma_{32}$). For the steady state the general solution of Eqns (4) has the form

$$N_1 = \left[\frac{Q_1}{\Gamma_1}\left(1 - \frac{A_{23}S_{32}}{\Gamma_2\Gamma_3}\right) + \frac{Q_2}{\Gamma_2}\frac{S_{21}}{\Gamma_1} + \frac{Q_3}{\Gamma_3}\frac{S_{21}S_{32}}{\Gamma_1\Gamma_2}\right] \times\left[1 - \frac{A_{12}S_{21}}{\Gamma_1\Gamma_2} - \frac{A_{23}S_{32}}{\Gamma_2\Gamma_3}\right]^{-1} = N_{10} + \delta N_1 \approx \frac{Q_1}{\Gamma_1} + \delta N_1,$$

$$N_2 = \left[\frac{Q_1}{\Gamma_1}\frac{A_{12}}{\Gamma_2} + \frac{Q_2}{\Gamma_2} + \frac{Q_3}{\Gamma_3}\frac{S_{32}}{\Gamma_2}\right]\left[1 - \frac{A_{12}S_{21}}{\Gamma_1\Gamma_2} - \frac{A_{23}S_{32}}{\Gamma_2\Gamma_3}\right]^{-1} = N_{20} + \delta N_2 \approx \frac{Q_2}{\Gamma_2} + \delta N_2,$$

$$N_3 = \left[\frac{Q_1}{\Gamma_1}\frac{A_{12}A_{23}}{\Gamma_2\Gamma_3} + \frac{Q_2}{\Gamma_2}\frac{A_{23}}{\Gamma_3} + \frac{Q_3}{\Gamma_3}\left(1 - \frac{A_{12}S_{21}}{\Gamma_1\Gamma_2}\right)\right] \times\left[1 - \frac{A_{12}S_{21}}{\Gamma_1\Gamma_2} - \frac{A_{23}S_{32}}{\Gamma_2\Gamma_3}\right]^{-1} = N_{30} + \delta N_3 \approx \frac{Q_3}{\Gamma_3} + \delta N_3.$$

For the corrections δN_1 and δN_2 to the stationary populations N_{10} and N_{20}, related to the variation of A_{23} and S_{32}, one can write the relation that directly follows from Eqn (4):

$$\delta N_1 = \frac{S_{21}}{\Gamma_1}\delta N_2.$$

The ratio of the resonance contrasts, obviously, is determined by the relation

* J_m, J_n are the total angular momenta of the upper and lower terms.

$$\frac{\delta N_1}{N_1} \Big/ \frac{\delta N_2}{N_2} \approx \frac{S_{21}\Gamma_1}{\Gamma_1 Q_1}\frac{\delta N_2}{\delta N_2}\frac{Q_2}{\Gamma_2} = \frac{Q_2}{Q_1}\frac{S_{21}}{\Gamma_2}.$$

For neon the typical situation is $Q_3 \gg Q_2 \gg Q_1$, $A_{12}/\Gamma_1 < 1$ and $A_{23}/\Gamma_2 < 1$. Then the contrast of the resonances at the transitions between the highly excited states can be much higher, and the attenuation of the radiation intensity, described by Eqn (3), can be practically absent due to the higher transparency of the medium for the natural spontaneous radiation at these transitions. It is worth noting that the growth of the OMR contrast will be observed not only at the transition n_1-n_2, but also at all transition from n_1 to all other levels. The sign of the resonance at the transition n_1-n_2 between higher excited states coincides with the sign of the resonance at the parent transition n_2-n_3. Between the levels of the multiplets 4d–2p, 3d–2p and 3s–2p, for which the high-contrast OMR-1200 were observed, and the levels $2p_5$, $2p_{10}$ and $1s_5$ the electric dipole transitions are allowed, which makes it possible to use the cascade scheme for interpretation. If this scheme is applied to the system of neon levels, then the transition n_1-n_2 is some of the transitions, belonging to the multiplets 4d–2p, 3d–2p or 3s–2p, and the level n_3 should be associated with the level $1s_5$.

When the dependences on the discharge current for the OMR-1200 amplitudes (Fig. 4a) are compared with those for the intensities of the corresponding spectral lines (Fig. 4d), a different behaviour is revealed. With the growth of current a monotonic increase in the line intensities is observed, while the OMR-1200 amplitude at first grows, reaches a maximum value, and then decreases. This behaviour is typical for the populations of the neon levels 1s and 2p [7–9]. Thus, the observation of high-contrast OMR-1200 at a number of transitions between highly excited neon levels does not contradict the hypothesis about their formation at the transitions $2p_5-1s_5$ (1225 Gs) and $2p_{10}-1s_5$ (1200 Gs).

Let us discuss the dependences shown in Figs 4b and 4c. For the resonances at all three lines a clearly seen regularity is a decrease in $|\Delta|$ with the growth of the current. In this case a tendency towards some decrease in the width of the resonance can be also noticed.

The considerable asymmetry of OMR-1200 with respect to the resonance value of Δ, well seen in Figs 2 and 3, indicates the fact that the major contribution to the signal is produced by the part of the discharge, located closer to the photodetector in the zone of non-uniform magnetic field, where $G_s(z)$ decreases. The decrease in $|\Delta|$ with increasing discharge current can be explained by the growth of the contributions to the signal from more remote regions, located in the zone of a more uniform magnetic field with large values of $G_s(z)$. The same mechanism causes some reduction of the width of resonances. It is worth paying attention to the relation between $|\Delta|$ and the intensity of the corresponding spectral line, namely, the value of $|\Delta|$ is smaller at the lines with smaller intensity.

Additional data about the properties of OMR-1200 can be extracted from the result of experiments with the use of an additional magnetic field. Assuming that the origin of OMR-1200 is related to the isotropic spontaneous radiation, one can perform a numerical calculation of the expected OMR shape with the real longitudinal profile of the magnetic field and the difference of contributions from different parts of the gas discharge cell into the OMR signal taken into account. The technique of the calculation is similar to that of Ref. [5] and consists in the use of Eqn (2) for the case when the magnetic field is produced by the scanned solenoid and the additional permanent magnet, and the DOMC is formed by the modulating solenoid:

$$I_d(H_z) = \int_0^L A_r(z)[\varphi(H_+) - \varphi(H_-)]\exp[-B_r(L-z)]\,dz,$$

$$\varphi(H) = \frac{\Gamma}{\Gamma^2 + (H-\Delta)^2}, \qquad (5)$$

$$H_\pm(z) = \sqrt{[H_z G_z(z) + h_z(z)]^2 + h_\perp^2(z)} \pm H_m(z).$$

Here $I_d(H_z)$ is the DOMC; $A_r(z)$ contains the additional dependence on the longitudinal coordinate due to a decrease in the contribution to $I_d(H_z)$ from the cell regions, remote from the photodetector (see Ref. [5]); H_z is the z-component of the magnetic field strength, proportional to the current in the scanned solenoid; $h_z(z)$ and $h_\perp(z)$ are the longitudinal and transverse components of the field produced by the additional permanent magnet; $H_m(z)$ is the field, produced by the modulating solenoid and proportional to $G_m(z)$; and $L = 400$ mm.

Equation (5) presents one of the implementations of the 'derivative method', in which the modulated field has the shape of a meander. At the values of $H_m(z)$ that do not exceed the narrow resonance width, such modulation is practically equivalent to the harmonic modulation of the magnetic field.

In Fig. 6a the calculated dependences of DOMC on H_z for $\Delta = 1200$ Gs are presented for different values of the non-selective absorption coefficient B_r. The solid lines plot the results of the calculation at $B_r = 0.001$ mm^{-1}, the dashed lines at $B_r = 0.01$ mm^{-1}. Curves (*1*) are calculated under the conditions when the additional magnet is absent; curves (*2*) and (*3*) correspond to the case, when the magnet is placed at the cell end nearer to the photodetector with different orientations [the configuration corresponds to curves (*2*) and (*3*) in Fig. 5]; and curves (*4*) and (*5*) correspond to the location of the magnet at the cell end far from the photodetector also with different orientations [the configuration corresponds to curve (*1*) in Fig. 5]. In Fig. 6b curve (*1*) corresponds to the profile of the unperturbed scanned magnetic field $G_s(z)$, curve (*6*) is the profile of the modulating magnetic field $G_m(z)$, and curves (*2–5*) show the profiles for the resulting scanned magnetic field with the field of the additional magnet taken into account. The profiles with the numbers *2–5* correspond to the plots of $I_d(H_z)$, denoted by numbers *2–5* in Fig. 6a. Curves (*7*) and (*8*) plot the dependences of the product $A_r(z)\exp[-B_r(L-z)]$ on z at $B_r = 0.001$ and 0.01 mm^{-1}, respectively.

In the absence of the additional magnet [curve (*1*) in Fig. 6a] the shape of the DOMC dependence resembles a Lorentzian derivative, centred near $H_z = 1200$ Gs. The dependence of the DOMC on H_z demonstrates breaking of symmetry with respect to the value $H_z = 1200$ Gs because of the longitudinal nonuniformity of the scanned magnetic field in the region of $G_s(z)$ and $G_m(z)$ overlap. The asymmetry of $I_d(H_z)$ increases with the growth of B_r. The effect is due to the growth of the contribution from the cell region nearer to the photodetector, where the nonuniformity of the magnetic field is mostly concentrated.

The addition of the field of the permanent magnet leads to the distortion of the profile of the scanned magnetic field. Depending on the orientation and position of the permanent magnet, its effect is reduced to the appearance of additional

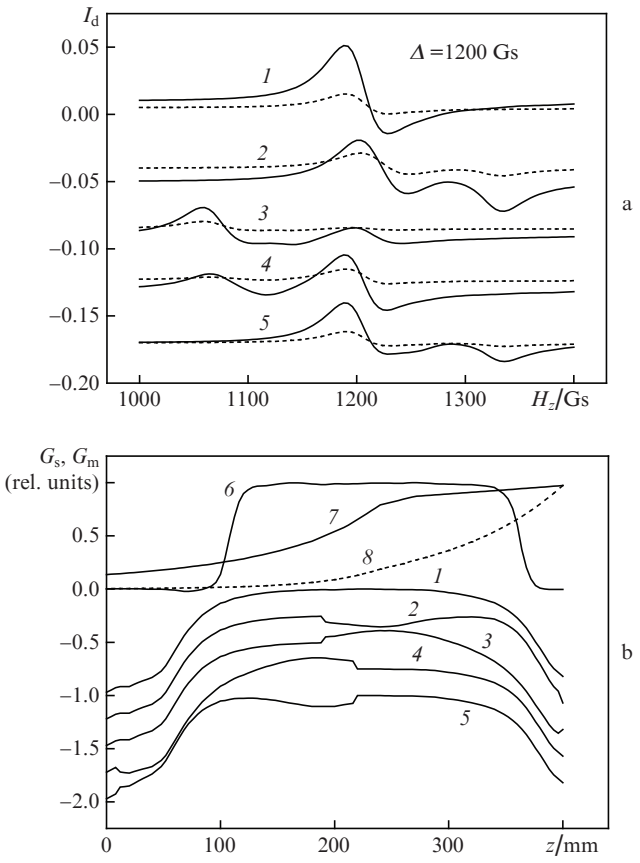

Figure 6. Calculated dependences of DOMC on H_z in the case of isotropic spontaneous emission for different profiles of the scanned magnetic field, modified by the field of the additional permanent magnet (a), as well as the profiles of the (*1*–*5*) scanned and (*6*) modulating magnetic field and the profiles $A_r(z)\exp[-B_r(L-z)]$ for B_r = (*7*) 0.001 and (*8*) 0.01 mm^{-1} (b).

resonances at 1320 Gs [curves (*2*) and (*5*) in Fig. 6a] or at 1080 Gs [curves (*3*) and (*4*) in Fig. 6a] in $I_d(H_z)$. The amplitudes of the additional resonances are greater, if the magnet is placed nearer to the photodetector. The appearance and position of the additional resonances are mainly related to the sign of $h_z(z)$. If there is a region of the scanned magnetic field profile, where $h_z(z)$ increases the projection of the summary filed on the z axis, then in $I_d(H_z)$ an additional structure arises at smaller values of H_z, and vice versa. The presence or absence of $h_\perp(z)$ in the resulting field does not affect noticeably the position of the additional structures in $I_d(H_z)$, but slightly changes their shape.

Curves (*2*–*5*) in Fig. 6a for B_r = 0.001 and 0.01 mm^{-1} differ only quantitatively. The growth of B_r leads to a decrease in the amplitude, the enhancement of $I_d(H_z)$ asymmetry, and smaller effect of the additional magnet placed at the cell end far from the photodetector.

The comparison of the experimental shape of OMR-1200 (see Fig. 5) with the results of calculation using Eqn (5) reveals essential qualitative difference. In the experimental observation of OMR-1200 the application of the magnet to the cell region nearer to the photodetector leads to a almost complete destruction of the narrow resonance. If the magnet is placed at the cell end far from the photodetector, it does not noticeably affect the OMR-1200 shape. Therefore, the OMR-1200 formation occurs in the cell region nearer to the photodetector. From the comparison of the profiles of $G_s(z)$ and $G_m(z)$ [curves (*1*) and (*6*) in Fig. 6b] it is seen that due to the particular construction of the electromagnet the $G_m(z)$ profile is shifted with respect to $G_s(z)$ towards the photodetector. Because of this fact the cell part nearer to the photodetector has a larger region, where $G_m(z)$ overlaps with $G_s(z)$ and the scanned magnetic field is nonuniform. In the cell part far from the photodetector the zone of such nonuniformity is essentially smaller. It follows that the OMR-1200 appear only in the zone of a nonuniform magnetic field.

The disappearance of OMR-1200 in curves (*2*) and (*3*) (Fig. 5) independent of the additional magnet orientation should be, probably, related to the effect of the field $h_\perp(z)$ that declines the resulting field vector from the z axis by 14°. If so, the spontaneous radiation of the isotopic pair of atoms, responsible for the formation of OMR-1200, would possess strong asymmetry of the directional pattern.

The predominant formation of OMR-1200 in the zone of the nonuniform magnetic field and the anisotropy of the emission directional pattern can be caused by the anisotropic excitation of the levels $2p_5$ and $2p_{10}$ of the 2p multiplet, from which the electric dipole transition to the metastable level $1s_5$ is allowed. Under the axial symmetry the anisotropy arises due to the fact that in the magnetic field with the strength ~1200 Gs the radiation, propagating along the direction of the magnetic field, for each of the circular polarisations is split into three non-overlapping spectral lines due to the anomalous Zeeman effect. The transition probability for each line is proportional to the square modulus of the Clebsh–Gordan coefficient

$$W(J_m, M_m, J_n, M_n, \sigma) \propto |\langle J_m M_m J_n - M_n | 1\sigma\rangle|^2$$
$$= |\langle J_m M_m J_n(-M_m + \sigma)|1\sigma\rangle|^2$$
$$= |\langle J_m(M_m + \sigma)J_n - M_n|1\sigma\rangle|^2.$$

Here M_m, M_n are the z-axis projections of J_m, J_n; and σ is the polarisation of radiation. For the transitions $2p_5-1s_5$ and $2p_{10}-1s_5$ with $J_m = 1$ and $J_n = 2$ the following relations hold

$$W(1,1,2,2,-1)/W(1,0,2,1,-1)/W(1,-1,2,2,-1)$$
$$= W(1,-1,2,-2,1)/W(1,0,2,-1,1)/W(1,1,2,0,1)$$
$$= 6/3/1.$$

This leads to the depletion of the magnetic sublevels with $M_m = \pm 1$ for each of the isotopes, and the transitions just from these sublevels possess the required value of the transition frequency difference and can be responsible for the formation of shifted OMR-1200. In fact, the phenomenon of optical pumping takes place from the sublevels $M_n = \pm 2$ of the metastable level $1s_5$. Only the appropriately polarised radiation from the sublevels with $M_m = 0$ of the upper level is able to return the population to the magnetic sublevels with $M_m = \pm 1$, and this radiation is strongly non-resonance in the uniform magnetic field. The nonuniformity of the magnetic field reduces this non-resonance property and facilitates the reverse pumping of atoms from the sublevels with $M_n = \pm 2$ of the metastable level to the sublevels with $M_m = \pm 1$, thus playing a positive role in the formation of OMR-1200. The level excitation anisotropy leads to significant anisotropy of the spontaneous emission, which is demonstrated by the experiments with the additional magnetic field.

5. Conclusions

The totality of experimental data presented in this paper show that the OMR-1200 observed in the emission of different spectral lines on neon, have the same origin. The transitions $2p_5-1s_5$ and $2p_{10}-1s_5$, having the isotope shifts 1225 and 1200 Gs, are the best candidates for the role of parent transitions (see Ref. [3]). The resonances manifest themselves in the reduction of the total glow of the discharge and insignificantly change the populations of the parent transitions.

The reabsorption of the intrinsic spontaneous radiation in the system of neon terms leads to the transfer of a part of population from the levels $1s_5$, $2p_5$, and $2p_{10}$ to higher excited levels, possessing essentially smaller equilibrium populations. The appearance of OMR-1200 with a significantly higher contrast at the spectral lines of the multiplets 4d–2p, 3d–2p and 3s–2p is associated with this circumstance.

The asymmetry of the OMR-1200 shape with respect to the resonance value of the magnetic field allows the conclusion that the resonances arise in the zone of longitudinal nonuniformity of the magnetic field. The experiments with additional transverse magnetic field provide a direct confirmation of this fact. Besides, it is found that the spontaneous radiation of the collective system, consisting of a pair of neon isotopes, has considerable anisotropy, with the directional pattern elongated in the direction of the magnetic field.

The obtained results fully agree with the hypothesis of the OMR-1200 formation as a result of crossing of the transition frequencies of different isotopes, possessing the anomalous Zeeman effect and interacting with the circularly polarised radiation. This hypothesis satisfactorily explains the origin of the OMR in the radiation, propagating presumably along the magnetic field direction, even under the conditions of isotropic excitation of degenerate levels. The excitation anisotropy, arising under the radiation trapping, additionally sharpens the directional pattern of the radiation, related to OMR.

In the present paper we paid absolutely no attention to the optical magnetic structures observed at small values of the magnetic field (±250 Gs). These structures are low-contrast, rather broad, and the additional transverse magnetic field affects them in a different way, changing only the position of resonances. Nevertheless, weakly shifted structures also have isotopic nature and are observed only in the mixture of neon isotopes (see Ref. [4]). Their properties, qualitatively different from those of high-contrast strongly-shifted OMR-1200, will be clarified in further studies.

It is worth paying attention to poorly understood asymmetry of the OMR-1200 amplitudes for different signs of the magnetic field. The asymmetry in the resonance amplitudes may attain 25% and is observed in all experiments. The intensities of the spectral lines, simultaneously measured with the photodetector for different signs of the magnetic field, differ by no more than 1%. This means that the considered asymmetry cannot be explained by the change of the position of the optical scheme elements under the action of the magnetic field of the scanned solenoid. Possibly it is caused by the additional transverse magnetic low-strength field, related to the field of the Earth, the field of the discharge current, or the field, arising due to magnetisation reversal in the elements of the experimental setup, made of steel.

Acknowledgements. The work was carried out within the framework of the State Project of Programme II.10.2 'Fundamental Problems of Interaction of Laser Radiation with Homogeneous and Structured Media' and under the support from the State Programme of Support of Leading Scientific Schools of the Russian Federation (Grant No. NSh-4447.2014.2).

References

1. Saprykin E.G., Sorokin V.A. *IV Int. Symp. 'Modern Problems of Laser Physics'* (Novosibirsk, 2004).
2. Saprykin E.G., Sorokin V.A. In: *Trudy IV mezhdunarodnoy konf. 'Problemy fundamental'noy optiki'* (Proc. IV INt. Conf. 'Problems of Fundamental Optics' (Saint-Petersburg, 2006) p. 175.
3. Saprykin E.G., Sorokin V.A., Shalagin A.M. *Zh. Eksp. Teor. Fiz.*, **143**, 622 (2013) [*JETP*, **116**, 541 (2013)].
4. Saprykin E.G., Sorokin V.A. *Opt. Spektrosk.*, **109**, 573 (2010) [*Opt. Spectrosc.*, **109**, 521 (2014)].
5. Saprykin E.G., Sorokin V.A. *Opt. Spektrosk.*, **117**, 20 (2014).
6. Striganov A.R., Sventitskii N.S. *Tablitsy spektral'nykh linii neytral'nykh i ionizirovannykh atomov* (Tables of Spectral Lines of Neutral and Ionised Atoms) (Moscow: Atomizdat, 1966).
7. Frish S.E. *Spektroskopiya gazorazryadnoi plazmy* (Spectroscopy of Gas-Discharge Plasma) (Leningrad: Nauka, 1970).
8. Penkin N.P. *Opt. Spektrosk.*, **2**, 545 (1957).
9. Penkin N.P. *Opt. Spektrosk.*, **23**, 878 (1967).